Dyes and Pigments 221 (2024) 111821

Contents lists available at ScienceDirect

Dyes and Pigments

journal homepage: www.elsevier.com/locate/dyepig

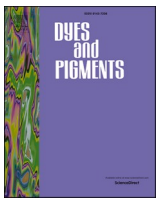

Photochemistry of a water-soluble coumarin-based photoswitch

Dóra Hessz [a,b], Etelka Kiss [a], Márton Bojtár [c], Attila Kunfi [d], Dávid Mester [a,b,e], Mihály Kállay [a,b,e], Miklós Kubinyi [a,*]

[a] Department of Physical Chemistry and Materials Science, Faculty of Chemical Technology and Biotechnology, Budapest University of Technology and Economics, 1111, Budapest, Műegyetem rkp. 3, Hungary
[b] MTA-BME Lendület Quantum Chemistry Research Group, Budapest University of Technology and Economics, 1111, Budapest, Műegyetem rkp. 3, Hungary
[c] Chemical Biology Research Group, Institute of Organic Chemistry, Research Centre for Natural Sciences, 1117, Budapest, Magyar Tudósok krt. 2, Hungary
[d] MTA-TTK Lendület Functional Organic Materials Research Group, Institute of Organic Chemistry, Research Centre for Natural Sciences, 1117, Budapest, Magyar Tudósok krt. 2., Hungary
[e] ELKH-BME Quantum Chemistry Research Group, Budapest University of Technology and Economics, 1111, Budapest, Műegyetem rkp. 3, Hungary

ARTICLE INFO

Keywords:
Charge transfer dye
Fluorescent photoswitch
Photoisomerization quantum yield
Photostationary state
Potential energy surface

ABSTRACT

A novel water-soluble stilbene-type molecular photoswitch (CP) has been synthesized by attaching an *N*-methylpyridinium unit to 7-diethylamino-4-methylcoumarin (coumarin 1) via an ethylene bridge. The photoisomerization cycle of CP and the spectroscopic properties of the two isomers were studied in acetonitrile and in water. In both solvents, the illumination of *trans*-CP with green light leads to a photostationary state (PSS) with 90% *cis* isomer and irradiating then this PSS mixture with near UV light, the *trans* isomer is almost fully recovered. In water, the quantum yield for the *trans-cis* photoisomerization is 0.042, for the *cis-trans* photoisomerization it is 0.23. In acetonitrile, the photoisomerization quantum yields are even higher, the respective values are 0.12 and 0.56. The *trans* isomer of CP is fluorescent with red emission and it has a large Stokes shift, whereas the *cis* isomer is non-fluorescent. The two isomers are thermally stable at room temperature. The efficient photoisomerization of CP in both direction, the thermal stability of both isomeric forms and the distinct fluorescence of the *trans* isomer suggest that some water-soluble coumarin-based photoswitches may be promising candidates for applications in fluorescence imaging of biological samples.

1. Introduction

Molecular photoswitches are systems of two isomeric molecules, the thermodynamically stable isomer can be converted into the metastable form by light irradiation. The return to the stable form can be induced by light of a different wavelength or simply by heat. The most widely known natural compound acting as a molecular photoswitch is 11-*cis*-retinal, which isomerizes into all-*trans*-retinal in the photochemical key reaction of vision [1]. Inspired by the natural photoswitches involved in some fundamental biological functions, scientists have developed a variety of synthetic photoswitches. Synthetic photoswitches have been successful in a variety of applications such as in molecular motors [2], photoelectronic devices [3], photoactuators [4], information encoding systems [5], solar energy stores [6,7], fluorescent biosensors [8], photocontrol of biological systems [9], photoswitchable catalysis [10] and photoactivable drugs [11–13].

Stilbenes, azobenzenes, spiropyrans, diarylethenes, fulgides and norbornadienes are some very popular classes of synthetic photoswitches [14,15]. By absorbing light of a suitable wavelength, stilbenes [16] and azobenzenes [17] undergo an *E-Z* isomerization [18], spiropyrans, fulgides and diarylethenes perform a ring-opening/closing reaction [19,20], whereas norbornadienes isomerize into quadricyclanes via an intramolecular cycloaddition [21].

Molecular photoswitches operable with visible light have backbones which are extensive conjugated systems with multiple bonds and aromatic units. Such structures are inherently lipophilic. With respect to the applications in biological systems (photoactivation of drugs, photocontrolling biological processes, fluorescent imaging of biological samples), there has been a continuous research effort to improve the water-solubility of photoswitching molecules [22]. The main strategies are to couple hydrophilic substituents to the hydrophobic structure, or, if there is a basic or acidic group in the photoswitch then to protonate the basic group or dissociate the acidic group by shifting the pH. Water-soluble photoswitches that can be reversibly cycled between a fluorescent and

* Corresponding author.
E-mail address: kubinyi.miklos@vbk.bme.hu (M. Kubinyi).

https://doi.org/10.1016/j.dyepig.2023.111821
Received 18 July 2023; Received in revised form 8 November 2023; Accepted 9 November 2023
Available online 11 November 2023

a non-fluorescent state are becoming particularly important tools in optical imaging techniques, involving super-resolution fluorescence microscopic methods [23]. Diraryl ethenes [24,25], spiropyrans [26] and spiropyran-naphthalimide FRET dyads [27] have been developed which showed photoswitchable on/off fluorescence in aqueous media.

In the present work, we studied the photoswitching properties of the coumarin derivative CP (see Fig. 1) which has a vinylpyridinium group in the 3-position. Coumarin dyes with various substituents attached via a vinylene bridge to the C3 atom of the coumarin core attract much interest for their diverse applications, such as fluorescent chemical sensors [28,29], fluorescent viscosity probes [30], dye sensitizers in solar cells [31], photocages [32,33] or dual color photoconverters [34]. The first coumarin based stilbene-type photoswitches (A1 and A2 in Fig. 2) have been described by Richers et al. [35]. They possessed a diethylamino electrondonor in the 7-position and one or two electron withdrawing cyano groups attached via an allylidene group to the 3-position of the coumarin scaffold. Irradiating them by green light in acetonitrile or DMSO solution, they underwent a *trans/cis* isomerization around the first exocyclic double bond and irradiating the *cis* product by near UV light the *trans* isomer could be recovered.

Our cationic photoswitch, CP, proved to be sufficiently soluble in water, allowing to study its photoisomerization cycle in aqueous solution. For comparison, its photoswitching behavior was also studied in acetonitrile. It was hoped that CP will be switchable between a bright and a dark state – using such fluorophores in biomaging, the interference by autofluorescence can be eliminated by optical modulation [36,37]. A further objective of our work was to explore the mechanism of the photoconversion reaction of CP on the basis of theoretical calculations. CP itself is a new compound, its analogue with a benzoate ester substituent (B in Fig. 2) acts as photocage, since irradiating it with visible light, it undergoes photohydrolysis. The caged benzoic acid moiety is released, leaving a 4-hydroxymethylcoumarin derivative as the other photoproduct [33].

2. Materials and methods

2.1. General

Commercial reagents, solvents and catalysts were purchased (Aldrich, Fluorochem, VWR) as reagent-grade and used without further purification. Solvents for extraction were of technical quality and were distilled for column chromatography. For spectroscopy and sample treatment opti-grade (spectroscopic grade) quality solvents were used. Organic solutions were concentrated by rotary evaporation at 25–40 °C. Thin layer chromatography was carried out on SiO_2–layered aluminum plates (60778-25 EA, Fluka). Column chromatography was performed using SiO_2–60 (230–400 mesh ASTM, 0.040–0.063 mm from Merck) at 25 °C or using a Teledyne Isco CombiFlash® Rf + automated flash chromatographer with silica gel (25–40 μm, Redisep Gold®). LC-MS analyses were performed on a Shimadzu LCMS-2020 System operated in electrospray ionization mode. Melting points were measured on a Stanford Research Systems – OptiMelt device.

The samples for the NMR, UV-VIS and fluorescence spectroscopic measurements were prepared under dimmed light conditions and they were kept in the dark until the beginning of the experiments. The NMR spectra were acquired on a Varian 500 NMR spectrometer.

The UV–Vis absorption spectra were recorded on an Agilent 8453 diode array spectrometer. The steady-state fluorescence spectra and the fluorescence decay curves were measured on an Edinburgh Instruments FS5 combined steady-state and lifetime spectrometer, which uses the method of time-correlated single-photon counting for measuring the fluorescence decay. The excitation light source was a Xe steady-state arc lamp when measuring the fluorescence spectra and an EPL 450 pulsed diode laser (emitting at 441 nm, pulse width ~ 100 ps) when the fluorescence decay curves were recorded. The fluorescence quantum yields were determined using Rhodamine 6G as reference (Φ_F= 0.94 in ethanol [38]). All the optical spectroscopic experiments were carried out at 25 °C.

2.2. Syntheses

2.2.1. Synthesis of 3-bromo-7-diethylamino-4-methylcoumarin (C1-Br)

C1-Br was synthesized as previously described in the literature [39].

2.2.2. Synthesis of 7-diethylamino-4-methyl-3-(2-(pyridin-2-yl)vinyl) coumarin (C1-vPyr)

C1-Br (100 mg, 0.322 mmol, 1 eq), 2-vinylpyridine (68 mg, 0.644 mmol, 2 eq), $Pd_2(dba)_3$ (28 mg, 0.032 mmol, 0.1 eq), QPhos (21 mg, 0.032 mmol, 0.1 eq) and *N,N*-dicyclohexylmethylamine (189 mg, 0.967 mmol, 3 eq) were dissolved in abs. DMF (2 mL) in a reactor tube under nitrogen atmosphere. In a microwave reactor the reaction mixture was stirred under continuous microwave irradiation to maintain 100 °C for 1 h. After completion, the mixture was dissolved in EtOAc (20 mL), filtered through a pad of Celite and the solvents were removed by rotary evaporation. The crude product was purified by flash column chromatography (hexane → hexane/EtOAc 1:1). The product was isolated as a yellow solid (100 mg, 93% yield). ^{1}H NMR (500 MHz, DMSO-d_6) δ 8.58 (d, J = 4.6 Hz, 1H), 7.82 (d, J = 15.7 Hz, 1H), 7.76 (td, J = 7.7, 1.8 Hz, 1H), 7.70 (d, J = 15.7 Hz, 1H), 7.67 (d, J = 9.2 Hz, 1H), 7.49 (d, J = 7.9 Hz, 1H), 7.25–7.21 (m, 1H), 6.74 (dd, J = 9.2, 2.6 Hz, 1H), 6.53 (d, J = 2.6 Hz, 1H), 3.45 (q, J = 7.0 Hz, 4H), 2.55 (s, 3H), 1.14 (t, J = 7.0 Hz, 6H). ^{13}C NMR (126 MHz, DMSO-d_6) δ = 159.46, 155.54, 154.29, 150.36, 149.83, 149.42, 136.73, 130.90, 127.06, 124.99, 122.60, 122.08, 113.35, 109.14, 108.84, 96.23, 43.99, 14.64, 12.33. ESI-MS *m/z*: $[MH]^+$ Calcd. for $C_{21}H_{23}N_2O_2$ 335.1760; Found 335.1743.

2.2.3. Synthesis of trans-CP

C1-vPyr (50 mg, 0.150 mmol, 1 eq) and iodomethane (280 μL, 4.50 mmol, 30 eq) were dissolved in dry MeCN (2 mL) and the reaction mixture was stirred at 80 °C for 18 h. The volatiles were removed under reduced pressure and the crude product was purified by flash column chromatography (DCM/MeOH 9:1). The product was isolated as an orange solid (64 mg, 90% yield). It was non-hygroscopic. ^{1}H NMR (500 MHz, CD_3CN) δ 8.50 (d, J = 6.3 Hz, 1H), 8.33 (d, J = 6.3 Hz, 2H), 8.16 (d, J = 15.4 Hz, 1H), 7.80 (d, J = 15.4 Hz, 1H), 7.74–7.66 (m, 2H), 6.78 (dd, J = 9.3, 2.6 Hz, 1H), 6.51 (d, J = 2.6 Hz, 1H), 4.20 (s, 3H), 3.49 (q, J

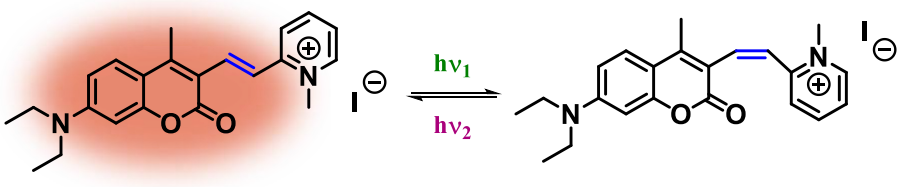

***trans*-CP** ***cis*-CP**

Fig. 1. Chemical structures of the isomers of photoswitch CP.

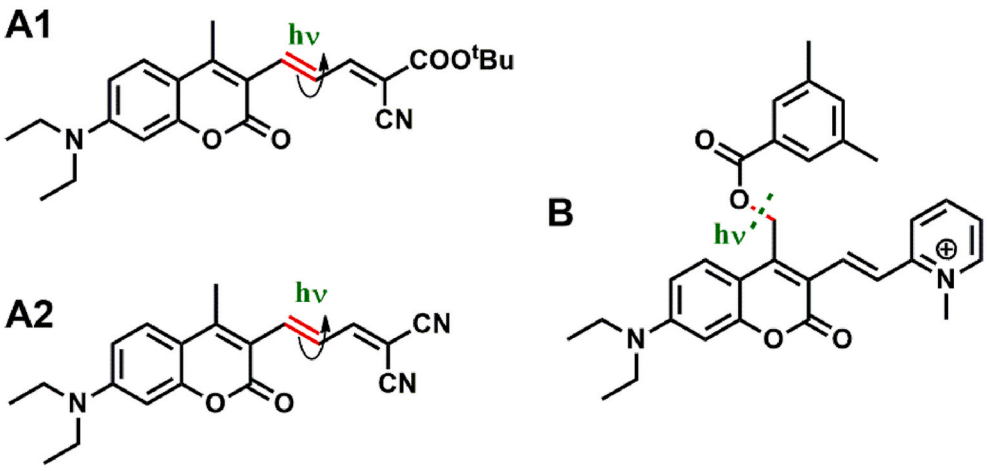

Fig. 2. Chemical structures of the coumarin-based photoswitches (A1, A2) described in Ref. [35] and the photocage (B) reported in Ref. [33].

= 7.1 Hz, 4H), 2.64 (s, 3H), 1.20 (t, $J = 7.1$ Hz, 6H). ^{13}C NMR (126 MHz, CD_3CN) δ 160.84, 156.81, 156.59, 155.36, 153.24, 146.27, 144.96, 137.72, 129.03, 126.02, 125.30, 118.87, 112.83, 110.84, 110.14, 97.33, 46.92, 45.55, 15.35, 12.76. ESI-MS *m/z*: $[MH]^+$ Calcd. for $C_{22}H_{25}N_2O_2$ 349.1916; Found 349.1923.

2.3. Photochemical experiments

The *trans*-to-*cis* isomerization of CP was achieved by illumination of solution samples with a 540 nm LED through a 550 nm low-pass (FGL550) filter, whereas the *cis*-to-*trans* isomerization was induced with a 370 nm LED. The kinetic experiments were carried out in a 1 cm quartz cell and the photoconversion was monitored by measuring the UV/VIS spectra of the samples. The photon fluxes in the kinetic experiments were determined by chemical actinometry, using $Ru(bpy)_3Cl_2$ based actinometry ($\Phi_{Ch} = 0.019$) in the visible range [40] and ferrioxalate actinometry [41] ($\Phi_{Ch} = 1$) in the near UV range. The actinometric measurements are described in the Supplementary Material.

2.4. Determination of the photoisomerization quantum yields

The quantum yields of the opposite photoisomerization reactions, $\Phi_{t\to c}$ and $\Phi_{c\to t}$ were determined from the time dependent absorbance data of the samples irradiated by the 540 nm and 370 nm LEDs (see section 2.3). The Beer-Lambert law for a system with the two isomers as absorbing species is

$$Abs(\lambda_D, \lambda_E, t) = \varepsilon_{trans}(\lambda_D) \bullet c_{trans}(\lambda_E, t) \bullet \ell + \varepsilon_{cis}(\lambda_D) \bullet c_{cis}(\lambda_E, t) \bullet \ell, \quad (1)$$

where $Abs(\lambda_D, \lambda_E, t)$ is the absorbance of the sample at detection wavelength λ_D, $\lambda_E (= \lambda_c$ or $\lambda_t)$ is the wavelength of the exciting light, $\varepsilon_{trans}(\lambda_D)$ and $\varepsilon_{cis}(\lambda_D)$ are the molar absorption coefficients of the isomers, ℓ is the optical path length. Supposing that no side product is formed, thus the mass balance is simply

$$c_{trans}(\lambda_E, t) + c_{cis}(\lambda_E, t) = c_{tot}. \quad (2)$$

where c_{tot} is the total concentration, one of the isomer concentrations can be eliminated from Eq (1),

$$Abs(\lambda_D, \lambda_E, t) = [\varepsilon_{trans}(\lambda_D) - \varepsilon_{cis}(\lambda_D)] \bullet c_{trans}(\lambda_E, t) \bullet \ell + \varepsilon_{cis}(\lambda_D) \bullet c_{tot} \bullet \ell \quad (3)$$

The time derivative of the isomer concentration, i. e. the reaction rate is related to the photoisomerization quantum yields. The reaction rate of a reversible photoisomerization reaction is [42].

$$-\frac{dc_{trans}(\lambda_E, t)}{dt} = \frac{\Phi_{t\to c} \bullet I(\lambda_E) \bullet \beta_{trans}(\lambda_E, t)}{N_A \bullet V} - \frac{\Phi_{c\to t} \bullet I(\lambda_E) \bullet \beta_{cis}(\lambda_E, t)}{N_A \bullet V} \quad (4)$$

where $I(\lambda_E)$ is the photon flux, N_A is the Avogadro number, V is the volume of the sample. $\beta_{trans}(\lambda_E, t)$ and $\beta_{cis}(\lambda_E, t)$ are the fractions of the absorbed light which have the forms

$$\beta_{trans}(\lambda_E, t) = \frac{\varepsilon_{trans}(\lambda_E) \bullet c_{trans}(\lambda_E, t)}{\varepsilon_{trans}(\lambda_E) \bullet c_{trans}(\lambda_E, t) + \varepsilon_{cis}(\lambda_E) \bullet c_{cis}(\lambda_E, t)} \left(1 - 10^{-Abs(\lambda_E, t)}\right) \quad (5a)$$

and

$$\beta_{cis}(\lambda_E, t) = \frac{\varepsilon_{cis}(\lambda_E) \bullet c_{cis}(\lambda_E, t)}{\varepsilon_{trans}(\lambda_E) \bullet c_{trans}(\lambda_E, t) + \varepsilon_{cis}(\lambda_E) \bullet c_{cis}(\lambda_E, t)} \left(1 - 10^{-Abs(\lambda_E, t)}\right) \quad (5b)$$

The isomerization quantum yields were obtained by a global fitting of simulated absorbance time profiles to the experimental data, with $\Phi_{t\to c}$ and $\Phi_{c\to t}$ as fitting parameters. The simulated absorbance profiles were calculated according to Eq (3), using $c_{trans}(\lambda_E, t)$ concentration functions generated by the numerical integration of the kinetic equation (4).

2.5. Computational methods

In the theoretical calculations, the Marvin [43] and the Gaussian 09 [44] program packages were used for the molecular mechanical (MM) and density functional theory (DFT) calculations, respectively. First, a MM conformation analysis was performed for both the *trans*- and *cis*-CP molecules, applying the MMFF94 [45] force field. For the stable conformers that were not more than 5 kcal/mol above the lowest energy conformer, the geometry was optimized further using the DFT method at the wB97X-D/6-311+G** level [46,47]. The excited-state calculations were carried out within the time-dependent DFT (TDDFT) formalism [48]. As demonstrated, the applied functional is one of the most suitable for calculating excitation energies [49], and its performance for ground-state properties is also outstanding [50]. Additionally, the selected basis set provides a reasonable compromise between accuracy and computational requirements. To mimic the experimental conditions, all (TD-)DFT calculations were performed using the polarized continuum model [51], with water and acetonitrile as the solvents. To obtain the ground- and excited-state potential energy surface (PES), constrained geometry optimizations were carried out. In these calculations, the torsional angle around the central C=C bond was fixed and all the other geometrical parameters were optimized.

3. Results and discussion

3.1. Synthesis of photoswitch CP

The synthetic route is shown in Fig. 3. The first step was the bromination of 7-(diethylamino)-4-methyl coumarin (coumarin 1, C1) at position 3 with *N*-bromosuccinimide [39]. This was followed by the extension of the electron system of the coumarin unit, which was accomplished by a Heck reaction with 2-vinylpyridine. The last step was the quaternization of the pyridine *N*-atom with methyl iodide, thus forming the strongly electron-withdrawing 3-vinyl-(2-pyridinium)-coumarin structure. The ^{1}H NMR spectrum indicated that the product was pure *trans* isomer. The solubility of CP in water was $3.6{\cdot}10^{-3}$ M at 25 °C.

3.2. Optical spectra of trans and cis isomers

In a preliminary experiment, a solution of *trans*-CP in acetonitrile was irradiated with the green LED and it caused spectacular changes in the appearance (see Fig. 4). Before the irradiation, the solution was orange in color. Under UV lamp, it exhibited a strong reddish-orange fluorescence. Following the irradiation, the color of the sample turned to yellow and its fluorescence was quenched almost completely.

The absorption spectra of *trans*-CP which was available in pure form, were taken in $2{\cdot}10^{-5}$ M solutions in acetonitrile and in water. The fluorescence spectra, fluorescence quantum yields and fluorescence lifetimes of *trans*-CP in the two solvents were measured in 10^{-6} M solutions.

To obtain the spectra of the *cis* form, photostationary mixtures were made by irradiating the solutions of the *trans* isomer with the 540 nm LED. In the fluorescence spectra of irradiated samples, no emission from the *cis* isomer was observed. Only the band of *trans*-CP appeared with a substantially decreased intensity, corresponding to 9% of the initial concentration in acetonitrile as well as in water. This result was confirmed by an NMR experiment (see Section 3.3). The relative intensities of the signals in the ^{1}H NMR spectrum of a photostationary mixture in CD_3CN also corresponded to a composition of 91% *cis* and 9% *trans* isomer. We note that at the photostationary state (PSS) the concentration ratio of the two isomers is given by

$$\left(\frac{c_{trans}}{c_{cis}}\right)_{PSS} = \frac{\Phi_{c\to t} \bullet \varepsilon_{cis}(\lambda_E)}{\Phi_{t\to c} \bullet \varepsilon_{trans}(\lambda_E)}. \tag{6}$$

(The relationship follows from Eq. (4) when the net reaction rate reaches zero.) This means that at the PSS, the isomeric ratio does not depend on the total concentration, thus, it will take the same value in the samples of very different total concentrations used in our fluorescence,

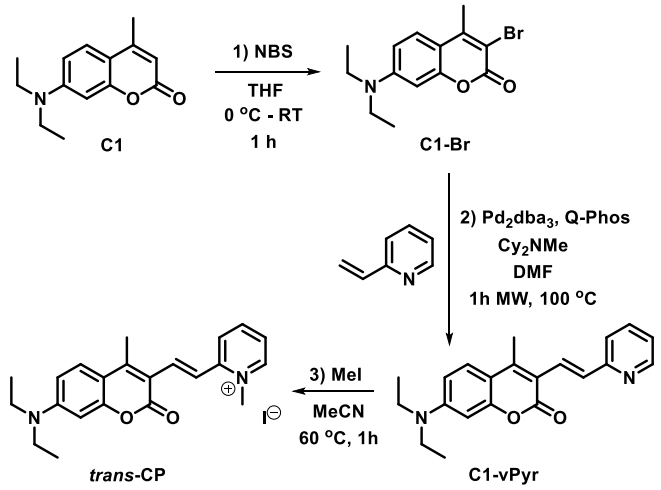

Fig. 3. Synthesis of the coumarin-based photoswitch CP.

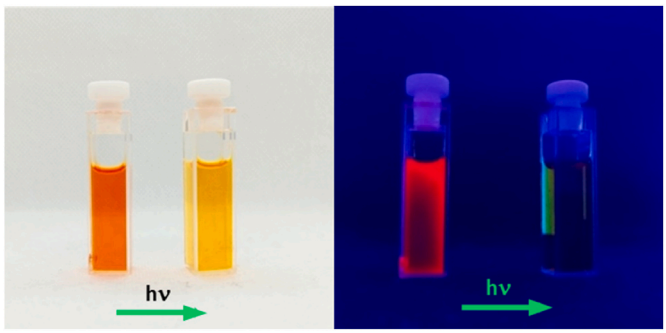

Fig. 4. Photographs of an acetonitrile solution of *trans*-CP before and after irradiation with the green LED; (left) photographs taken in daylight, (right) photographs taken under UV light.

UV-VIS absorption and NMR experiments.

Following the determination of the isomeric ratios in the photostationary mixtures, the absorption spectra of *cis*-CP in the two solvents were obtained by decomposing the spectra of the mixtures with *cis* isomer excesses as the weighted sums of the spectra of the pure isomers. This is illustrated in Fig. S3 in the Supplementary Material where the spectrum of the photostationary mixture in acetonitrile is resolved into the spectra of the two isomers.

The absorption spectra of the two isomers and the fluorescence spectrum of *trans*-CP in acetonitrile and in water are shown in Fig. 5. The wavelengths of the LED-s used for irradiation are indicated in the figure. As can be seen, at 370 nm the *cis* isomer absorbs much stronger than the *trans* isomer, whereas at 540 nm practically only the *trans* isomer shows absorption, the absorption of the *cis* isomer is negligible. Irradiating the samples at these wavelengths, photostationary mixtures with high isomeric excesses could be obtained.

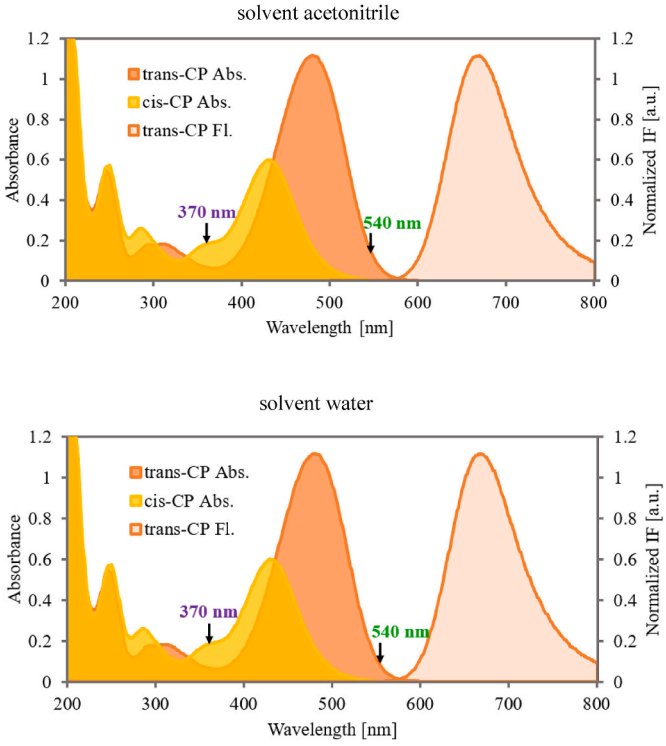

Fig. 5. Absorption spectra of *trans*-CP and *cis*-CP and the fluorescence spectra of *trans*-CP in acetonitrile and in water. The concentrations are $2{\cdot}10^{-5}$ M (absorption spectra) and 10^{-6} M (fluorescence spectra). The fluorescence spectra were obtained with excitation at 540 nm. The arrows note the wavelengths of the LED-s used for irradiation.

The spectral data of the two isomers are collected in Table 1. For comparison, the data of the parent compound C1 are also presented in the table.

Comparing the spectral data of *trans*-CP and the parent compound C1, it can be seen that the absorption band as well as the fluorescence band of *trans*-CP show a significant redshift, as a consequence of the extended conjugated system. In addition, the Stokes shift of *trans*-CP is even larger than the Stokes shift of C1, indicating that the positively charged substituent in *trans*-CP enhances the strong CT character of the parent C1 molecule further.

The fluorescence quantum yields of C1 and *trans*-CP are lower in water than in acetonitrile. Water is a general quencher, due to a resonant energy transfer process, in which the electronic excitation energy of fluorescent solutes is transformed to the energy of the high frequency overtones and combinations of the water solvent molecules [54]. In addition, coumarin fluorophores with rotatable dialkylamino groups, like C1 and *trans*-CP, also deactivate via a highly polar dark TICT state and this process is preferred in the highly polar water solvent [52,53] The fluorescence quantum yields of *trans*-CP are lower in both solvents than the respective Φ_F values of C1. This in accordance with the ability of the excited *trans*-CP molecule to isomerize which is an additional deactivation channel. *Cis*-CP is non-fluorescent, like the *cis* isomers of many other stilbene-like molecules [55–58].

The *cis* isomer of the stilbene parent molecule is very weakly fluorescent at room temperature, whereas the fluorescence of *trans*-stilbene is relatively strong. ($\Phi_F^{cis} = 1.2 \bullet 10^{-4}, \Phi_F^{trans} = 0.055$ in hexane) [59]. According to a widely used model for the photoinduced processes in stilbene, the non-radiative $S_1 \rightarrow S_0$ decays of the two isomers, leading to partial isomerization, proceeds via a common intermediate with perpendicular conformation, called p^* or 'phantom' state [60–62]. Starting from the *trans* isomer, the molecules pass over a 3 kcal/mol barrier before reaching the p^* state, whereas from the *cis* isomer the rotation to the p^* state is barrierless, minimizing the probability of fluorescence emission [60,61]. Comprehensive theoretical calculations on the photochemistry of stilbene found non-radiative decay pathways via conical intersections, with a barrier only on the side of *trans*-stilbene [63].

3.3. NMR spectra of trans and cis isomers

The ^{1}H NMR spectra of *trans*-CP and a photostationary mixture were taken in 10 mg/ml CD_3CN solutions. The latter sample was obtained by irradiating the *trans* isomer with the 540 nm LED light for ~20 min (A higher photon flux was applied than in the UV-VIS experiments.) The obtained mixture was kept in the dark until the NMR measurement. Some characteristic ranges of the spectra are shown in Fig. 6.

The main difference between the spectra of the two isomers is shown by the signals of the protons on the central C=C bond where the photoisomerization takes place. In the spectrum of *trans*-CP, the pair of doublets showing "roof effect" belong to these two protons, they appear at 7.80 ppm and 8.16 ppm, with a coupling constant of 15.4 Hz. The respective signals are shifted upfield by ~1 ppm in the spectrum of *cis*-CP and the coupling constant is significantly smaller, 11.9 Hz.

In the spectrum of the irradiated sample, the relative intensities of the *trans* isomer correspond to ~9% molar concentration. This is illustrated in Fig. 6 by the 2.4–2.7 ppm ranges of the spectra where the signals of the 4-methyl groups of the two isomers can be seen.

The complete NMR spectra of the *trans* isomer and the photostationary mixture with the *cis* isomer in excess are shown in Figs. S2 and S4 in the Supplementary Material.

3.4. Photoisomerization cycle

The photoisomerization cycles in acetonitrile and water were studied by irradiating $2{\cdot}10^{-5}$ M solutions of *trans*-CP in the two solvents with the 540 nm LED until a stationary state was reached and subsequently, irradiating the samples with the 370 nm LED until another stationary state was achieved. The temporal variation of the absorption spectra in the two solvents are shown in Fig. 7. As written in section 3. 2., the photostationary mixtures rich in the *cis* isomer consisted of 91% *cis* and 9% *trans* isomer in both solvents. The subsequent back isomerization induced by the 370 nm LED was much faster and the stationary mixtures contained >99 % *trans* isomer.

The quantum yields of the opposite photoisomerization reactions $\Phi_{t\rightarrow c}$ and $\Phi_{c\rightarrow t}$ were determined from the time dependent absorbances at 540 nm, as described in Section 2.4. The results are presented in Table 2. As can be seen, for the excited state *cis* isomer, the photoisomerization is the main route of deactivation. The quantum yields for the *trans-cis* isomerization are lower – the excited *trans* isomer also deactivates via fluorescence emission. The $\Phi_{t\rightarrow c}$ and $\Phi_{c\rightarrow t}$ values measured in water are lower than the respective values measured in acetonitrile. This can be explained by the same reasons as the lower fluorescence quantum yield observed in water: the quenching effect of the water matrix and a decay route via a highly polar TICT state. But even if the reaction rates are lower in water, the photoactive compound can be switched efficiently between two stationary states at which the mixture contains the *trans* or the *cis* isomer at high excesses.

The different rates in the *trans-cis* and *cis-trans* directions, shown by the different absorption time profiles in Fig. 7, can be interpreted in terms of the rate equation, Eq (4) in Section 2.4. As shown by Eq (4), the rate of the net reaction in the irradiated samples depends on the quantum yields of the opposing photoreactions, on the light flux of the irradiating beam and - via the fractional absorptions – on the absorption coefficients of the two isomers at the irradiation wavelength. The absorption coefficients at 370 nm are related as $\varepsilon_{cis} \gg \varepsilon_{trans}$, promoting the *cis-trans* isomerization, whereas at 540 nm they are related as $\varepsilon_{trans} \gg \varepsilon_{cis}$, favoring the *trans-cis* conversion. The faster *cis*-to-*trans* isomerization achieved by the UV LED was caused partly by the higher photon flux incident on the sample. This value was $4.52{\cdot}10^{-9}$ (mol photon)/s when the 370 nm LED was the irradiating source and $1.07{\cdot}10^{-9}$ (mol photon)/s when the 540 nm LED (with filter) was used for irradiation. The other reason of the faster *cis*-to-*trans* isomerization was the difference in the photoisomerization quantum yields, $\Phi_{c\rightarrow t} \gg \Phi_{t\rightarrow c}$, the excited *trans*-CP molecules also relax radiatively to their ground state.

The thermal stability of the two photoisomers was tested by measuring at intervals the UV-VIS spectra of the PSS mixtures kept in the dark at room temperature. The spectra did not show detectable changes

Table 1
Photophysical properties of coumarin dyes C1, *trans*-CP and *cis*-CP.

solvent	compound	λ_{abs} [nm]	ε [$M^{-1}cm^{-1}$]	λ_F [nm]	Φ_F [−]	τ_F [ns]	Stokes shift [cm^{-1}]
acetonitrile	C1[a]	367		438	0.62	3.24	4259
	trans-CP	481	44600	618	0.091	0.375	4610
	cis-CP	432	24000	non-fl.	–	–	–
water	C1[b]	385		470	0.041	0.36	4697
	trans-CP	472	24600	618	0.011	<0.02	5005
	cis-CP	441	15000	non-fl.	–	–	–

[a] Ref. [52].
[b] Ref. [53].

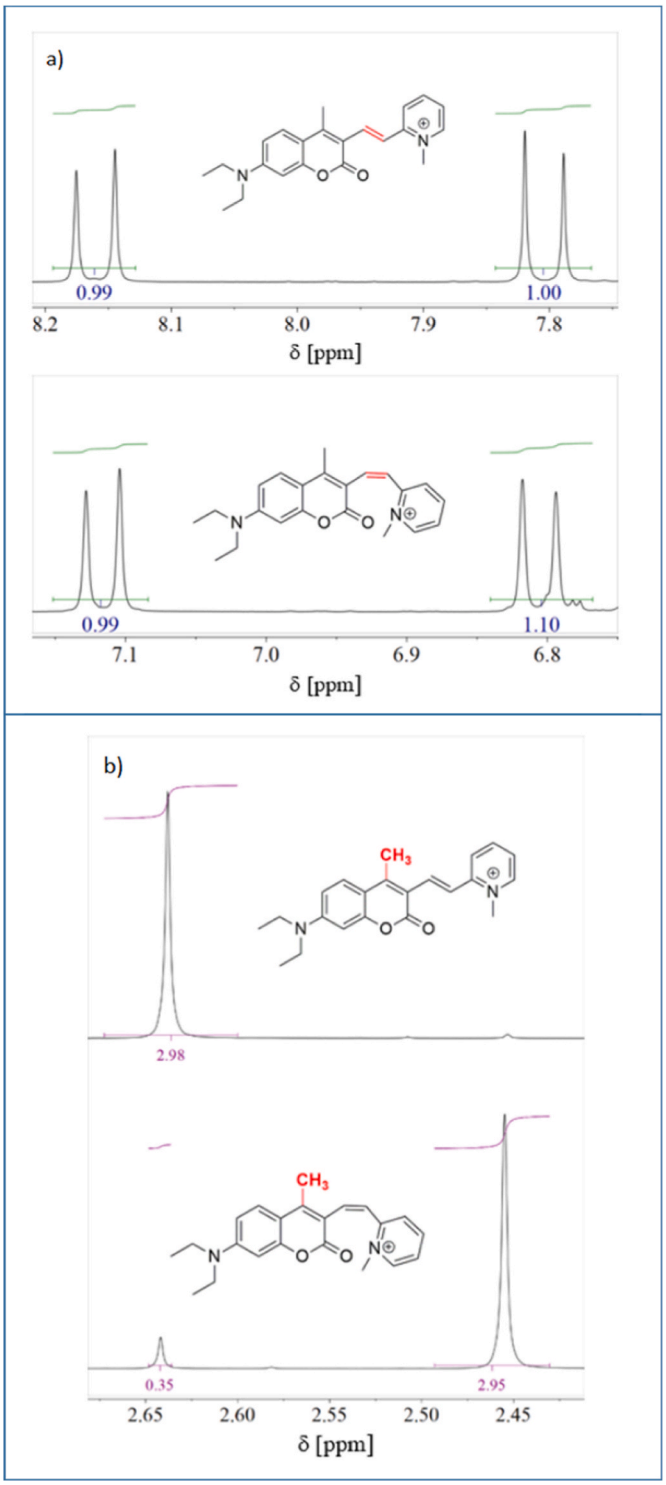

Fig. 6. Ranges of the ^{1}H NMR spectra (500 MHz, CD_3CN) of *trans*-CP and a photostationary mixture in which *cis*-CP is the dominant isomer. (a) Signals of the protons on the central C=C bond, (b) signal of the 4-methyl group.

for three days, proving that both *trans*-CP and *cis*-CP are thermally stable in acetonitrile and in aqueous solution (see Fig. S5 in Supplementary Material).

We also tested the fatigue behavior of the molecular photoswitch CP, applying repetitive irradiations with the 370 nm and 540 nm LEDs. As can be seen in Fig. 8, there was a small, but observable decrease in the signal amplitude with the number of isomerization cycles, CP showed a fairly good, but not complete resistance to photofatigue.

3.5. Potential energy surface calculations

The potential energy surfaces for the ground state and excited state *trans-cis* isomerization of CP, calculated for aqueous solution, are visualized in Fig. 9. The surfaces were obtained by constrained geometry optimizations in which the twisting angle around the ethylenic C=C bond was fixed and all the other geometrical parameters were optimized.

Inspecting the ground state surface, the *cis* isomer has minimally higher energy than the *trans* isomer, the difference is less than 1 kcal/mol. The two isomers are, however, separated by a high (~30 kcal/mol) activation barrier, located at a twisting angle of 90°. These findings confirm that both isomers are thermally stable in their ground states.

The calculations indicate the existence of two conical intersections (CI1 and CI2) between the ground state and excited state surfaces. For the *trans*-to-*cis* photoisomerization the pattern of PES diagram suggests a route on which the molecule relaxes to the ground state surface at CI1, the conical intersection around 60° and it reaches then the TS where the molecule has perpendicular conformation. The subsequent relaxation on the ground state surface branches – it leads both to *cis*-CP and *trans*-CP molecules. The *cis*-to-*trans* photoisomerization proceeds in an analogous manner. The excited *cis*-CP molecule decays to the ground state PES at CI2, the conical intersection around 120°, it relaxes then to the TS from where the route branches to the ground state *trans* and *cis* isomers.

The excited *trans*-CP molecule reaches the CI on its side via a barrier of 6 kcal/mol, whereas for *cis*-CP this barrier height is only 1 kcal/mol. Therefore, the non-radiative deactivation of the excited *trans* isomer is expected to be much slower and the *trans* isomer is expected to produce a much stronger fluorescence than the *cis* isomer. This is in accordance with the observation that only the *trans* isomer of CP emits detectable fluorescence.

On the excited-state PES there is a shallow local minimum at a twisting angle of 90°, above TS state, the local maximum on the ground state surface. This minimum corresponds to the 'phantom' (p^*) state of stilbene and related molecules [64]. In addition to the reaction paths via the CI stationary points, the *trans*-to-*cis* as well as the *cis*-to-*trans* isomerization may also take place via the p^* and TS states.

The substantial difference between the dynamics of the thermal and photoinduced isomerization reactions can also be rationalized in terms of the bond lengths in the central ethylene unit. For the ground-state *trans*-CP molecule, the length of the double bond is 1.348 Å, while the lengths of the single bonds connecting the vinylpyridinium group and the coumarin moiety to the ethylene unit are 1.455 and 1.451 Å, respectively. In the transition state on the ground state surface, the double bond elongates to 1.419 Å, while the single bonds shorten to 1.406 and 1.398 Å, respectively. In other words, the lengths of the bonds move significantly closer to each other. In the excited state *trans*-CP molecule, the length of the former double bond is 1.403 Å, while the lengths of the former single bonds are 1.407 and 1.401 Å, respectively. This structure with the three practically equivalent bonds favors the torsional motion of the substituents around the central bond, leading to isomerization. Similar findings can be made comparing the ground and excited state structures of the *cis* form.

The calculations for the photoisomerization reactions of CP in acetonitrile produced qualitatively similar results. The corresponding surfaces are presented in Fig. S6 in the Supplementary Material.

4. Conclusion

We studied the photoisomerization cycle of a stilbene type molecular photoswitch, CP in acetonitrile and in water. CP consists of a diethylamino-coumarin and an *N*-methylpyridinium moiety which are linked via a vinylene bridge. The *trans* isomer is fluorescent with a large Stokes shift and emission in the red range, whereas the *cis* isomer is non-emissive. CP can be switched efficiently between the two isomeric states in both solvents. The *trans*-to-*cis* isomerization can be induced by green

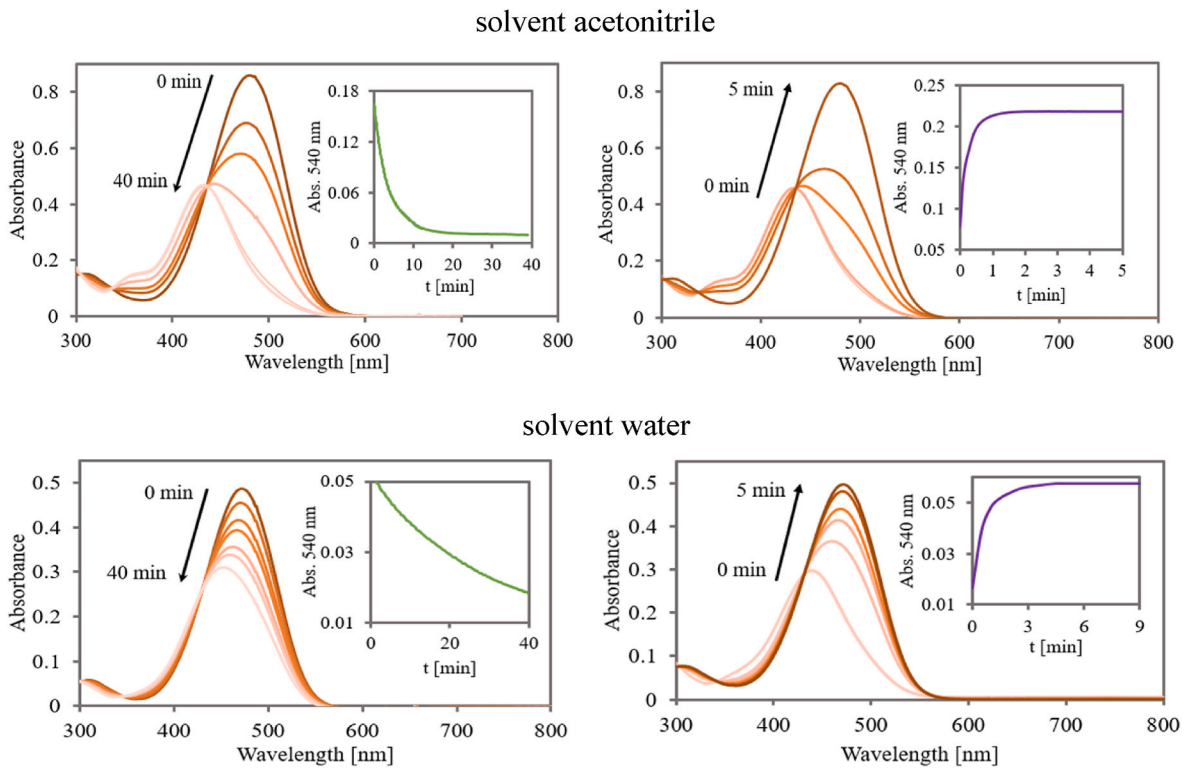

Fig. 7. Photoinduced variations of the absorption spectra of CP in $2{\cdot}10^{-5}$ M solutions in acetonitrile and water. (left) The solutions of *trans*-CP are irradiated by the green LED, (right) the photostationary mixtures with 91 % *cis*-CP are irradiated with the near UV LED. The insets show the change of the absorbance at 540 nm.

Table 2
Photoisomerization quantum yields of photoswitch CP.

Solvent	$\Phi_{t\rightarrow c}$	$\Phi_{c\rightarrow t}$
acetonitrile	0.12	0.56
water	0.042	0.23

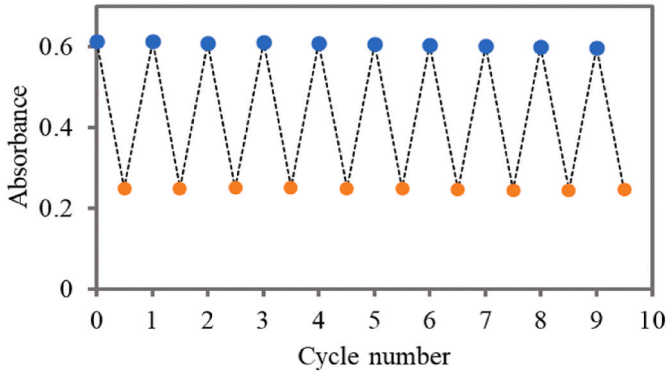

Fig. 8. Evolution of the absorbance at 472 nm of a $2{\cdot}10^{-5}$ M CP solution in water during repetitive switching cycles consisting of consecutive visible (540 nm, 70 s) and UV (370 nm, 4 s) irradiations.

light, the *cis*-to-*trans* isomerization can be achieved via irradiation with near UV light. For the *trans*-to-*cis* isomerization the quantum yields are lower than for the reverse process, in accordance with the fluorescence of *trans*-CP which competes with the isomerization in the deactivation of the excited molecule. The photoisomerization quantum yields are lower in water than in acetonitrile. Presumably, this is related to a deactivation route via a non-emissive TICT state which is more stable in the highly polar water. Even higher photoisomerization quantum yields can be

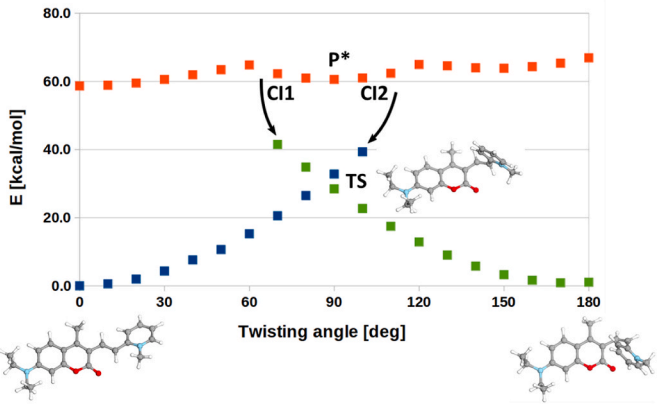

Fig. 9. The ground-state (blue and green squares) and excited-state (orange squares) PES-s of the CP molecule along the torsion of the central C=C double bond. TS is the transition state on the ground state surface, CI1 and CI2 are conical intersections, p^* is the 'phantom' state. Solvent: water.

hoped from analogue coumarin-based photoswitches with amino groups fused with the coumarin core, however, such coumarin derivatives are expected to be more hydrophobic.

The efficient photoisomerization of CP in both direction, the thermal stability of both isomeric forms and the distinct fluorescence of the *trans* isomer suggest that such type water-soluble coumarin-based photoswitches may be promising candidates for applications in fluorescence imaging of biological samples.

CRediT authorship contribution statement

Dóra Hessz: Methodology, Resources, Investigation. **Etelka Kiss:** Investigation, Formal analysis, Visualization. **Márton Bojtár:**

Investigation, Validation. **Attila Kunfi:** Investigation, Writing – original draft. **Dávid Mester:** Formal analysis, Writing – original draft. **Mihály Kállay:** Formal analysis, Funding acquisition. **Miklós Kubinyi:** Conceptualization, Project administration, Writing – original draft.

Declaration of competing interest

The authors declare that they have no known competing financial interests or personal relationships that could have appeared to influence the work reported in this paper.

Data availability

Data will be made available on request.

Acknowledgement

The authors are grateful to Zsófia Puskás for her contribution to the photochemical experiments.

This work has been supported by the Ministry of Culture and Innovation of Hungary from the National Research, Development and Innovation Fund, under the TKP2021-NVA funding scheme (Project no. TKP-6-6/PALY-2021). Further financial support by the National Research, Development and Innovation Office, Hungary (Grants PD-135121, PD-137866, PD-142372, ÚNKP-22-4-II-BME-157, ÚNKP-23-4-II-BME-275, KKP126451) and the Lendulet Program of the Hungarian Academy of Sciences (LENDULET_2018-355) is gratefully acknowledged.

Appendix A. Supplementary data

Supplementary data to this article can be found online at https://doi.org/10.1016/j.dyepig.2023.111821.

References

[1] Ernst OP, Lodowski DT, Elstner M, Hegemann P, Brown LS, Kandori H. Microbial and animal rhodopsins: structures, functions, and molecular mechanisms. Chem Rev 2014;114:126–63. https://doi.org/10.1021/cr4003769.
[2] Lubbe AS, Liu Q, Smith SJ, de Vries JW, Kistemaker JCM, de Vries AH, Faustino I, Meng ZJ, Szymanski W, Herrmann A, Feringa BL. Photoswitching of DNA hybridization using a molecular motor. J Am Chem Soc 2018;140:5069–76. https://doi.org/10.1021/jacs.7b09476.
[3] Goulet-Hanssens A, Eisenreich F, Hecht S. Enlightening materials with photoswitches. Adv Mater 2020;32(2020):1905966. https://doi.org/10.1002/adma.201905966.
[4] Boelke J, Hecht S. Designing molecular photoswitches for soft materials applications. Adv Opt Mater 2019;7:1900404. https://doi.org/10.1002/adom.201900404.
[5] Gentili PL, Bartolomei B, Micheau J-C. Light-driven artificial neuron models based on photoswitchable systems. Dyes Pigments 2021;187:109086. https://doi.org/10.1016/j.dyepig.2020.109086.
[6] Losantos R, Sampedro D. Design and tuning of photoswitches for solar energy storage. Molecules 2021;26:3796. https://doi.org/10.3390/molecules26133796.
[7] Sun CL, Wang CX, Boulatov R. Applications of photoswitches in the storage of solar energy. Chemphotochem 2020;3:268–83. https://doi.org/10.1002/cptc.201900030.
[8] Bierbuesse F, Bourges AC, Gielen V, Mönkemöller V, Vandenberg W, Shen Y, Hofkens J, Vanden Berghe P, Campbell RE, Moeyaert B, Dedecker P. Absolute measurement of cellular activities using photochromic single-fluorophore biosensors and intermittent quantification. Nat Commun 2022;13:1850. https://doi.org/10.1038/s41467-022-29508-w.
[9] Szymanski W, Beierle JM, Kistemaker HAV, Velema WA, Feringa BL. Reversible photocontrol of biological systems by the incorporation of molecular photoswitches. Chem Rev 2013;113:6114–78. https://doi.org/10.1021/cr300179f.
[10] Kunfi A, Jablonkai I, Gazdag T, Mayer PJ, Kalapos PP, Németh K, Holczbauer T, London G. A photoresponsive palladium complex of an azopyridyltriazole ligand: light-controlled solubility drives catalytic activity in the Suzuki coupling reaction. RSC Adv 2021;11:23419–29. https://doi.org/10.1039/D1RA03838A.
[11] Borowiak M, Nahaboo W, Reynders M, Nekolla K, Jalinot P, Hasserodt PJ, Rehberg M, Delattre M, Zahler S, Vollmar A, Trauner D, Thorn-Seshold O. Photoswitchable inhibitors of microtubule dynamics optically control mitosis and cell death. Cell 2015;162:403–11. https://doi.org/10.1016/j.cell.2015.06.049.
[12] Izquierdo-Serra M, Bautista-Barrufet A, Trapero A, Garrido-Charles A, Díaz-Tahoces A, Camarero N, Pittolo S, Valbuena S, Pérez-Jiménez A, Gay M, García-Moll A, Rodríguez-Escrich C, Lerma J, de la Villa P, Fernández E, Pericàs MÀ, Llebaria A, Gorostiza P. Optical control of endogenous receptors and cellular excitability using targeted covalent photoswitches. Nat Commun 2016;7:1221. https://doi.org/10.1038/ncomms12221.
[13] Matera C, Gomila AMJ, Camarero N, Libergoli M, Soler C, Gorostiza P. Photoswitchable antimetabolite for targeted photoactivated chemotherapy. J Am Chem Soc 2018;140:15764–73. https://doi.org/10.1021/jacs.8b08249.
[14] Pianowski ZL. Recent implementations of molecular photoswitches into smart materials and biological systems. Chem Eur J 2019;25:5128–44. https://doi.org/10.1002/chem.201805814.
[15] Leistner AL, Pianowski ZL. Smart photochromic materials triggered with visible light. Eur J Org Chem 2022:e202101271. https://doi.org/10.1002/ejoc.202101271.
[16] Coelho PJ, Cidalia M, Castro R, Manuela M, Raposo M. Fast (hetero)aryl-benzothiazolium ethenes photoswitches activated by visible-light at room temperature. Dyes Pigments 2015;117:163–9. https://doi.org/10.1016/j.dyepig.2015.02.015.
[17] Dudek M, Pokladek Z, Deiana M, Matczyszyn K. Molecular design and structural characterization of photoresponsive azobenzene-based polyamide units. Dyes Pigments 2020;180:108501. https://doi.org/10.1016/j.dyepig.2020.108501.
[18] Cameron D, Eisler S. Photoswitchable double bonds: synthetic strategies for tunability and versatility. J Phys Org Chem 2018;31:1–10. https://doi.org/10.1002/poc.3858.
[19] Buback J, Kullmann M, Langhojer F, Nuernberger P, Schmidt R, Würthner F, Brixner T. Ultrafast bidirectional photoswitching of a spiropyran. J Am Chem Soc 2010;132:16510–9. https://doi.org/10.1021/ja1062746.
[20] Li ZY, He CJ, Lu ZQ, Li PS, Zhu YP. Recent progress in all-visible-light-triggered diarylethenes. Dyes Pigments 2020;182:108623. https://doi.org/10.1016/j.dyepig.2020.108623.
[21] Orrego-Hernandez J, Dreos A, asper Moth-Poulsen K. Engineering of norbornadiene/quadricyclane photoswitches for molecular solar thermal energy storage applications. Acc Chem Res 2020;53:1478–87. https://doi.org/10.1021/acs.accounts.0c00235.
[22] Volaric J, Szymanski W, Simeth NA, Feringa BL. Molecular photoswitches in aqueous environments. Chem Soc Rev 2021;50:12377–449. https://doi.org/10.1039/d0cs00547a.
[23] Olesinska-Mönch M, Deo C. Small-molecule photoswitches for fluorescence bioimaging: engineering and applications. Chem Commun 2023;59:660–8. https://doi.org/10.1039/d2cc05870g.
[24] Um SH, Kim HJ, Kim D, Kwon JE, Lee JW, Hwang D, Kim SK, Park SY. Highly fluorescent and water soluble turn-on type diarylethene for super-resolution bioimaging over a broad pH range. Dyes Pigments 2018;158:36–41. https://doi.org/10.1016/j.dyepig.2018.05.014.
[25] Qiu SL, Frawley AT, Leslie KG, Anderson HL. How do donor and acceptor substituents change the photophysical and photochemical behavior of dithienylethenes? The search for a water-soluble visible-light photoswitch. Chem Sci 2023;14:9123–35. https://doi.org/10.1039/D3SC01458D.
[26] Halbritter T, Kaiser C, Wachtveitl J, Heckel A. Pyridine-spiropyran derivative as a persistent, reversible photoacid in water. J Org Chem 2017;82:8040–7. https://doi.org/10.1021/acs.joc.7b01268.
[27] Zhang JJ, Fu YX, Han HH, Zang Yi, Li J, He XP, Feringa BL, Tian H. Remote light-controlled intracellular target recognition by photochromic fluorescent glycoprobes. Nat Commun 2017;8:987. https://doi.org/10.1038/s41467-017-01137-8.
[28] Yuan L, Lin WY, Yang YT, Song JZ, Wang JL. Rational design of a highly reactive ratiometric fluorescent probe for cyanide. Org. Lett. 2011;13:3730–3. https://doi.org/10.1021/ol2013928.
[29] Yuan L, Lin WY, Yang YT. A ratiometric fluorescent probe for specific detection of cysteine over homocysteine and glutathione based on the drastic distinction in the kinetic profiles. Chem Commun 2011;47:6275–7. https://doi.org/10.1039/C1CC11316J.
[30] Singh D, Regar R, Soppina P, Soppina V, Kanvah S. Imaging of lipid droplets using coumarin fluorophores in live cells and *C. elegans*. J Photochem Photobiol B 2022;237:112589. https://doi.org/10.1016/j.jphotobiol.2022.112589.
[31] Martins S, Avo J, Lima J, Nogueira J, Andrade L, Mendes A, Pereira A, Branco PS. Styryl and phenylethynyl based coumarin chromophores for dye sensitized solar cells. J Photochem Photobiol 2018;353:564–9. https://doi.org/10.1016/j.jphotochem.2017.12.018.
[32] Lin QN, Yang LP, Wang ZQ, Hua YJ, Zhang DS, Bao BK, Bao CY, Gong XQ, Zhu LY. Coumarin photocages modified with an electron-rich styryl moiety at the 3-position: long wavelength excitation, rapid photolysis and photobleaching. Angew Chem Int Ed 2018;130:3784–8. https://doi.org/10.1002/ange.201800713.
[33] Bojtár M, Kormos A, Kis-Petik K, Kellermayer M, Kele P. Green-light activatable, water-soluble red-shifted coumarin photocages. Org Lett 2018;21:9410–4. https://doi.org/10.1021/acs.orglett.9b03624.
[34] Saladin L, Dal Pra O, Klymchenko AS, Didier P, Collot M. Tuning directed photooxidation-induced conversion of pyrrole-based styryl coumarin dual-color photoconverters. Chem Eur J 2023;29:202203933. https://doi.org/10.1002/chem.202203933.
[35] Richers MT, Du Tran D, Wachtveitl J, Ellis-Davies GCR. Coumarin-diene photoswitches for rapid and efficient isomerization with visible light. Chem Commun 2018;54:4983–6. https://doi.org/10.1039/c8cc01091a.
[36] Chouket R, Pellissier-Tanon A, Lemarchand A, Espagne A, Le Saux T, Jullien L. Dynamic contrast for overcoming spectral interferences in fluorescence imaging. J. Phys. Photonics 2020;2:032003. https://doi.org/10.1088/2515-7647/ab9099.

[37] Jung HY, Kim B, Jeon MH, Kim Y. Reversible near-infrared fluorescence photoswitching in aqueous media by diarylethene: toward high-accuracy live optical imaging. Small 2022;18:2103523. https://doi.org/10.1002/smll.202103523.
[38] Fischer M, Georges J. Fluorescence quantum yield of rhodamine 6G in ethanol as a function of concentration using thermal lens spectrometry. Chem Phys Lett 1996;260:115–8. https://doi.org/10.1016/0009-2614(96)00838-X.
[39] Supporting information for H. M. Guo, F.tanaka, A fluorogenic aldehyde bearing a 1,2,3-triazole moiety for monitoring the progress of aldol reactions. J Org Chem 2009;74:2417–24. https://pubs.acs.org/doi/suppl/10.1021/jo900013w/suppl_file/jo900013w_si_001.pdf.
[40] Pitre SP, McTiernan CD, Vine W, DiPucchio R, Grenier M, Scaiano JC. Visible-light actinometry and intermittent illumination as convenient tools to study Ru(Bpy)3Cl2 mediated photoredox transformations. Sci Rep 2015;5:16397. https://doi.org/10.1038/srep16397.
[41] Hatchard CG, Parker CA. A new sensitive chemical actinometer - II. Potassium ferrioxalate as a standard chemical actinometer. Proc Roy Soc Lond A 1956;235:518–36. https://doi.org/10.1098/rspa.1956.0102.
[42] Stranius K, Börjesson K. Determining the photoisomerization quantum yield of photoswitchable molecules in solution and in the solid state. Sci Rep 2017;7:41145. https://doi.org/10.1038/srep41145.
[43] Marvin 23.4.0, ChemAxon. 2023. http://www.chemaxon.com.
[44] Frisch MJ, Trucks GW, Schlegel HB, Scuseria GE, Robb MA, Cheeseman JR, Scalmani G, Barone V, Mennucci B, Petersson GA, Nakatsuji H, Caricato M, Li X, Hratchian HP, Izmaylov AF, Bloino J, Zheng G, Sonnenberg JL, Hada M, Ehara M, Toyota K, Fukuda R, Hasegawa J, Ishida M, Nakajima T, Honda Y, Kitao O, Nakai H, Vreven T, Montgomery Jr JA, Peralta JE, Ogliaro F, Bearpark M, Heyd JJ, Brothers E, Kudin KN, Staroverov VN, Kobayashi R, Normand J, Raghavachari K, Rendell A, Burant JC, Iyengar SS, Tomasi J, Cossi M, Rega N, Millam JM, Klene M, Knox JE, Cross JB, Bakken V, Adamo C, Jaramillo J, Gomperts R, Stratmann RE, Yazyev O, Austin AJ, Cammi R, Pomelli C, Ochterski JW, Martin RL, Morokuma K, Zakrzewski VG, Voth GA, Salvador P, Dannenberg JJ, Dapprich S, Daniels AD, Farkas Ö, Foresman JB, Ortiz JV, Cioslowski J, Fox DJ. Gaussian 09, revision B.01. Wallingford CT: Gaussian, Inc.; 2010.
[45] Halgren TA. MMFF VI. MMFF94s option for energy minimization studies. J Comput Chem 1999;20:720–9. https://doi.org/10.1002/(SICI)1096-987X(199905)20:7<720::AID-JCC7>3.0.CO;2-X.
[46] Chai J, Head-Gordon M. Long-range corrected hybrid density functionals with damped atom–atom dispersion corrections. Phys Chem Chem Phys 2008;10:6615–20. https://doi.org/10.1039/B810189B.
[47] Krishnan R, Binkley JS, Seeger R, Pople JA. Self-consistent molecular orbital methods. XX. A basis set for correlated wave functions. J Chem Phys 1980;72:650–4. https://doi.org/10.1063/1.438955.
[48] Casida ME, Huix-Rotllant M. Progress in time-dependent density-functional theory. Annu Rev Phys Chem 2012;63:287–323. https://doi.org/10.1146/annurev-physchem-032511-143803.
[49] Liang J, Feng X, Hait D, Head-Gordon M. Revisiting the performance of time-dependent density functional theory for electronic excitations: assessment of 43 popular and recently developed functionals from rungs one to four. J Chem Theor Comput 2022;18:3460–73. https://doi.org/10.1021/acs.jctc.2c00160.
[50] Goerigk L, Hansen A, Bauer C, Ehrlich S, Najibi A, Grimme S. A look at the density functional theory zoo with the advanced GMTKN55 database for general main group thermochemistry, kinetics and noncovalent interactions. Phys Chem Chem Phys 2017;19:32184–215. https://doi.org/10.1039/c7cp04913g.
[51] Miertus E Scrocco, Tomasi J. Electrostatic interaction of a solute with a continuum. A direct utilization of ab initio molecular potentials for the prevision of solvent effects. Chem Phys 1981;55:117–29. https://doi.org/10.1016/0301-0104(81)85090-2.
[52] Barik A, Nath S, Pal H. Effect of solvent polarity on the photophysical properties of coumarin-1 dye. J Chem Phys 2003;119:10202–8. https://doi.org/10.1063/1.1619933.
[53] Barik A, Kumbhakar M, Nath S, Pal H. Evidence for the TICT mediated nonradiative deexcitation process for the excited coumarin-1 dye in high polarity protic solvents. Chem Phys 2005;315:277–85. https://doi.org/10.1016/j.chemphys.2005.04.018.
[54] Maillard J, Klehs K, Rumble C, Vauthey E, Heilemann M, Fürstenberg A. Universal quenching of common fluorescent probes by water and alcohols. Chem Sci 2021;12:1352–62. https://doi.org/10.1039/d0sc05431c.
[55] Mishra A, Thangamani A, Chatterjee S, Chipem FAS, Krishnamoorthy G. Photoisomerization of *trans*-2-[4′-(Dimethylamino)styryl]benzothiazole. Photochem Photobiol 2012;89:247–52. https://doi.org/10.1111/j.1751-1097.2012.01227.x.
[56] Jedrzejewska B, Osmialowski B, Zalesny R. Application of spectroscopic and theoretical methods in the studies of photoisomerization and photophysical properties of the push–pull styryl-benzimidazole dye. Photochem Photobiol Sci 2016;15:117–28. https://doi.org/10.1039/c5pp00361j.
[57] Budyka MF, Li VM. Visible-light-driven two-way photoisomerization of 1-(1-pyrenyl)-2-(2-quinolyl)ethylene in neutral and protonated forms. Photochem Photobiol Sci 2018;17:213–20. https://doi.org/10.1039/c7pp00359e.
[58] Hsu YF, Hong JW, Yang JS. A highly fluorescent cis-stiff-stilbene. ChemPhotoChem 2023;7:e202200185. https://doi.org/10.1002/cptc.202200185.
[59] Sajadi M, Dobryakov AL, Garbin E, Ernsting NP, Kovalenko SA. Time-resolved fluorescence spectra of *cis*-stilbene in hexane and acetonitrile. Chem Phys Lett 2010;489:44–7. https://doi.org/10.1016/j.cplett.2010.02.034.
[60] Saltiel J, Waller AS, Sears Jr DF, Garrett CZ. Fluorescence quantum yields of *trans*-Stilbene-d_0 and $-d_2$ in n-hexane and *n*-tetradecane. Medium and deuterium isotope effects on decay processes. J Phys Chem 1993;97:2516–22. https://doi.org/10.1021/j100113a009.
[61] Saltiel J, Waller AS, Sears Jr DF. The temperature and medium dependencies of *cis*-stilbene fluorescence. The energetics for twisting in the lowest excited singlet state. J Am Chem Soc 1993;115:2453–65. https://doi.org/10.1021/ja00059a047.
[62] Nakamura T, Takeuchi S, Taketsugu T, Tahara T. Femtosecond fluorescence study of the reaction pathways and nature of the reactive S1 state of *cis*-stilbene. Phys Chem Chem Phys 2012;14:6225–32. https://doi.org/10.1039/C2CP23959K.
[63] Tomasello G, Garavelli M, Orlandi G. Tracking the stilbene photoisomerization in the S1 state by RASSCF. Phys Chem Chem Phys 2013;15:19763–73. https://doi.org/10.1039/C3CP52310A.
[64] Williams M, Forbes R, Weir H, Veyrinas K, MacDonell RJ, Boguslavskiy AE, Schuurman MS, Stolow A, Martinez TJ. Unmasking the *EEE*-stilbene phantom state via vacuum ultraviolet time-resolved photoelectron spectroscopy and ab initio multiple spawning. J Phys Chem Lett 2021;12:6363–9. https://doi.org/10.1021/acs.jpclett.1c01227.